Finite element simulation of 0°/90° CFRP laminated plates subjected to crushing using a free-face-crushing concept

H.A. Israr [a,b], S. Rivallant [a,*], C. Bouvet [a], J.J. Barrau [a]

[a] Université de Toulouse: ISAE, INSA, UPS, Emac, ICA (Institut Clement Ader), ISAE, 10 Avenue Edouard Belin, BP 54032, 31055 Toulouse Cedex 4, France
[b] Faculty of Mechanical Engineering, Universiti Teknologi Malaysia, 81310 UTM Skudai, Johor, Malaysia

A B S T R A C T

This paper describes the development of a numerical model of (0°/90°) CFRP plates subjected to low velocity crushing, based on physical observations. The developed model is represented at the meso-scale and is based on five main ideas: 1 – meshing of each ply of the laminate; 2 – use of cohesive elements to represent delamination and plies splaying; 3 – simulation of macro-scale fragments; 4 – representation of the localized crushing of plies at their extremities with the introduction of a free-face-crushing concept; 5 – representation of contacts between plies, plies and impacted base, plies and debris. The results of the Abaqus/Explicit simulations show a good agreement with the experimental results, which demonstrates that the proposed methodology is able to predict the force, the main failure mechanisms and the phenomenology observed during experiments. Furthermore, an analysis of the repartition of absorbed energies is done, which shows that the most efficient mechanism is the localized crushing in the 0° plies.

Keywords:
A. Carbon fiber
B. Fragmentation
C. Computational modeling
Crushing

1. Introduction

The use of composite materials in vehicles structural design is increasing significantly which requires a comprehensive understanding of their behavior when subjected to crash loads. The aim is to demonstrate their ability to maintain the same level of safety and crashworthiness as compared to conventional materials. Therefore many studies on composite crashworthiness have been done for the last 30 years with a wide range of knowledge and information gained concerning their crushing behavior.

However, in recent years [1–6], the interest in crashworthiness studies focus more on the development of numerical modeling resulting from the availability of better computational resources and new explicit finite element codes in order to replace the high cost experimental works. The numerical modeling of composite crashworthiness was initiated in 1989 [7]. Starting from that point, many efforts have been made by many researchers to improve the numerical modeling of composite crashworthiness in various aspects such as the choice of constitutive models [3,4], delamination techniques [4] and triggering mechanisms [5] in order to predict with accuracy the crushing morphology, specific energy absorption (SEA) and force–displacement curve, as observed experimentally. However, the complex nature of fracture behaviors in crushing makes them difficult to be predicted numerically. These behaviors are highly dependent on many parameters such as geometry, laminate sequences, mechanical properties, contact and friction [7,8]. Thus, the capability of existing numerical models to describe the initiation and progression of a crushing mode right up to the point of final failure is still limited.

Crush phenomenon in composites generally involves failure modes different from those observed in conventional metallic materials which take place at different length scales [8]. Hence, limitations in numerical models can also result from the choice of modeling scales to predict the crushing mechanisms. Some of the models developed in the past [2–5,9,10] are based on global test characterizations (macro-scale) making the model strongly dependent on the laminate behavior. Even though this methodology makes modeling simpler and decreases computational time, but it cannot represent the damage mechanisms that takes place at sub-ply scale.

Concerning models using micro-scale approach, physical representation of such a complex phenomenon is difficult, and even if it is possible, detailed physical parameters and internal variables concerning each kind of damage involved [11] are needed which are very difficult to obtain. Furthermore, it requires high computational time that would restrain study cases only to small structures.

* Corresponding author. Address: ISAE/DMSM, 10 Avenue Edouard Belin, BP 54032, 31055 Toulouse Cedex 4, France. Tel.: +33 561338158; fax: +33 561338352.
E-mail addresses: haris@fkm.utm.my (H.A. Israr), samuel.rivallant@isae.fr (S. Rivallant), christophe.bouvet@isae.fr (C. Bouvet).

Between these two scales, the meso-scale approach, commonly used in composite modeling [12], seems to be the appropriate one. Although it requires more detailed laws as compared to macro-scale models, it nonetheless has the potential to capture most of the physical phenomena occurring at the crushing front [1].

A challenge in composite crashworthiness modeling is to be able to predict crushing damage modes, their evolution during crushing, and the energy absorption. This paper describes the development of a numerical modeling for carbon fiber reinforced plastic (CFRP) laminated plates subjected to crushing. The modeling methodology presented is based on numerous physical observations made during experimental crushing tests of composite plates [13–15]. Results of these observations enabled to determine the appropriate scale (ply scale or meso-scale), to numerically represent the mechanical phenomena involved in the progressive crushing of composite plates.

To adequately describe the crushing morphology in the numerical modeling which involves large deformation, the use of non-linear analyses via an explicit code is recommended along with suitable damage models [6]. Most of the damage models used in crushing modeling are based on conventional failure criterions with varying degrees of success in simulating crushing behaviors in composite structures. However, in this work an unconventional damage model is used to develop a meso-scale numerical model in order to represent the mixed-mode crushing (fragmentation and splaying) including the modeling of localized crushing at the extremity of the plies in fragmentation mode and at the same time other failures that might occur away from the plate extremity during progressive crushing. Details of the failure modes, constitutive laws and the numerical modeling strategy are explained in this paper. All parameters required in this model are elementary material characteristics, identified at the ply scale.

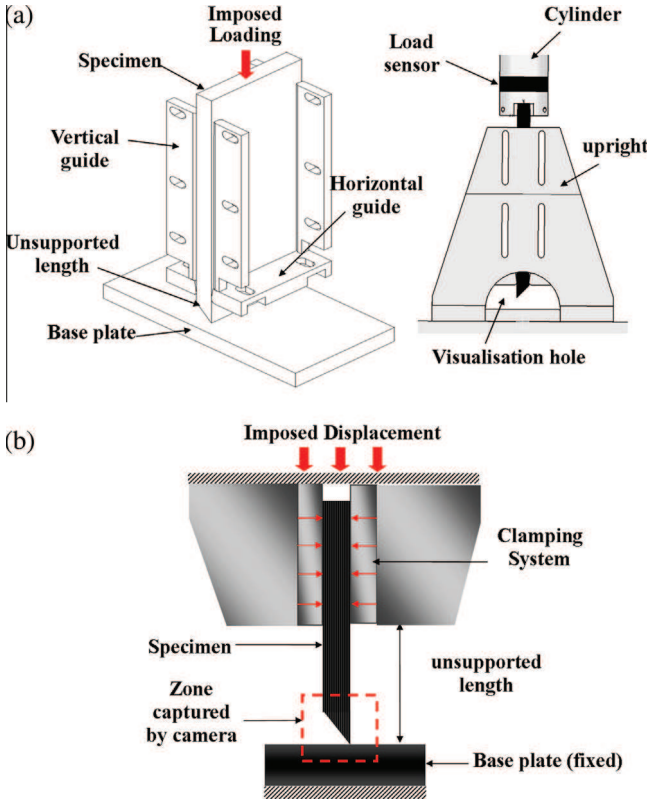

Fig. 1. Test fixture: (a) dynamic plate test (b) medium-scale quasi-static test. (For interpretation of the references to colour in this figure legend, the reader is referred to the web version of this article.)

2. Experiments

2.1. Specimen and test set-up

Two types of experimental tests taken from previous studies [13–15] are used to observe damage mechanisms involved in low velocity crushing of plates for the development of the numerical model and also for validation purpose. For each configuration, the experimental tests are carried out twice. The same type of specimen but with different dimensions is used in both tests. These specimens are 16 ply laminates $[(0°/90°)_4]_s$ made of T700/M21 carbon epoxy UD prepregs and the ply thickness is 0.26 mm. One end of each specimen is cut to form a 45° chamfer trigger (Fig. 1).

The first kind of test is a dynamic plate crushing test performed using a drop tower with a 9 m/s initial speed and a 36 kg falling weight. The specimens are 160 mm × 60 mm flat plates. The test fixture of this test is shown in Fig. 1a [13,14]. The unsupported length was fixed to 20 mm and is constant throughout the crushing test. The design of this test fixture enables introducing constant boundary conditions across the whole width of the crushing front. As a result, the visible edges of the plate are representative of the crushing phenomenon in the whole width. The use of high speed cameras allows a real-time visualization of the crushing front during the initiation and propagation of damage and allows correlations with the force–displacement curve. The image acquisition speed is 20,000 frames per second, with a 40 pixels per mm resolution. Detailed explanations of this test can be found in [13,14].

The second test is a medium-scale quasi-static crushing test on smaller specimens: 60 mm length and 10 mm width. This test is performed using a hydraulic testing machine in compression, at a 6 mm/min constant speed. The unsupported length is set to 30 mm and decreases as the imposed displacement increases. Cameras are also used to observe precisely the crushing mechanisms (1 Hz acquisition, 100 pixels per mm). Fig. 1b shows this test set-up, and test details are available in [15].

Apart from that, additional observations are also made from micro-scale quasi-static crushing tests performed inside a scanning electron microscope (SEM), on the same laminates (but smaller specimens), to investigate details of the micro-mechanisms. High quality images of the front geometry are obtained during all tests to support a physical observation work in order to develop a phenomenological model.

2.2. Damage mechanisms

Due to the chamfer trigger at one end of the plate, most of the specimens experienced crushing under a combination of fragmentation and splaying. Generally, during crushing one can observe three main kinds of damage in both tests (dynamic or static) as shown in Fig. 2 and described in the following sections.

2.2.1. Splaying

Early in the crushing process, ply interfaces at the tip of the specimens are subjected to high stresses. This leads to delamination and then splaying of plies. The proportion of plies that bend on each side is variable. Initiation and propagation of delamination can occur either in pure opening (mode I), shear (mode II) or more often in a combination of these two modes.

2.2.2. Fragmentation

Plies that do not turn to the splaying mode undergo fragmentation which occurs at two different scales.

The first scale is a fragmentation localized at the tip of the plies. In 0° plies, localized fragmentation is due to micro-buckling of

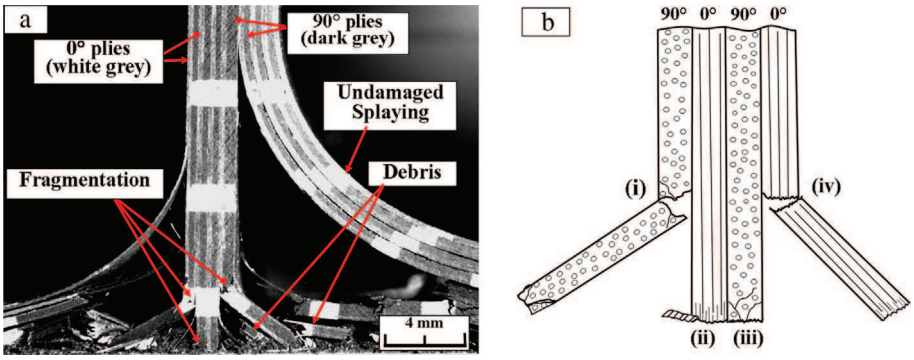

Fig. 2. (a) Major kinds of damage in mixed-mode crushing *(Note: white painted stripes are used to follow the plate displacement)* (b) fragmentation modes: (i) inside ply matrix cracking (ii) 0° localized crushing (iii) 90° localized crushing (iv) inside ply fiber breakage. (For interpretation of the references to colour in this figure legend, the reader is referred to the web version of this article.)

fibers near the contact surface between plies and the metallic base as illustrated in Fig. 2b (case ii). In 90° plies, the localized fragmentation is due to multiple shear micro-cracks at the tip of the plies as shown in Fig. 2b (case iii) and Fig. 3. This localized fragmentation (both in 0° and 90° plies) is the mechanism leading to the definition of the ply mean crushing stress (MCS) presented in [15]. In this paper, it will be called localized crushing.

The second level of fragmentation is the one induced by classical intra-laminar ply failure, fiber breakage and matrix cracks due to a combination of compression, bending and shear, but it is not localized at the tip of the plies (Fig. 2b case i and iv). In this paper, it will be called inside ply failure to differentiate from the localized crushing previously described.

2.2.3. Debris accumulation

These different kinds of failures occurring at the crushing front generate different sizes of fragments or debris.

The size of fragments created by localized crushing in 0° plies is under 0.25 mm (Fig. 2b case ii and Fig. 3). In 90° plies, localized crushing develops multiple micro-cracks that can lead to a macro-crack through the whole thickness of the ply, and consequently to larger fragments having size from 0 to 0.5 mm as observed in Fig. 3.

On the contrary, in the case of inside ply failure fragmentation for both 0° and 90°, because failure occurs further from the extremity of the ply, the debris are bigger: from 0.5 mm to 5 mm as shown in Fig. 2a and illustrated in Fig. 2b (case i and iv). Besides that, fragments made of 0° and 90° plies attached together can also be observed.

The accumulation of fragments can create a debris wedge during the crushing process, which can change the evolution of the crushing front. Unfortunately, from experimental observations, it seems that the slipping (and evacuation) or accumulation of debris is quite random. Debris due to localized crushing in 90° plies can have a particular role in the crushing process. Fig. 3 shows the formation of a trapezoidal wedge at the tip of a 90° ply. The shape of this wedge, with a 45° angle crack, and its confinement between 0° plies instigates a transverse load on the 0° neighboring plies that leads to the delamination of one of the 0°/90° interfaces. If the transverse force is high enough, it can initiate the splaying of one of the 0° plies. If this is not the case, the 0° ply will be subjected to localized crushing.

3. Numerical modeling

3.1. Finite element model

Numerical models of the previously described tests – medium-scale quasi-static (FEM static) and dynamic plate crushing tests

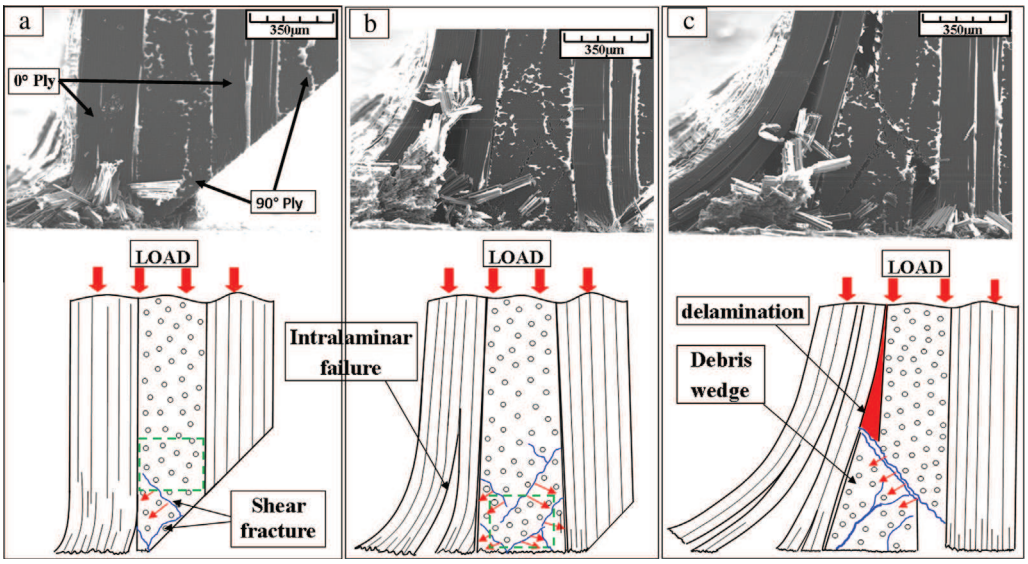

Fig. 3. Creation of a debris wedge in a 90° ply: SEM in situ test. (For interpretation of the references to colour in this figure legend, the reader is referred to the web version of this article.)

(FEM dynamic) – have been developed in Abaqus/Explicit. Taking into account the experimental observations, the choice of the model scale is essential for accurate representation of the mechanisms involved in the development and the propagation of a crushing front in laminates. Because all mechanisms (fragmentations, splaying, fiber ruptures, debris accumulation, etc.) occur at the scale of the ply, it will be considered as the scale for the model (meso-scale). Therefore, each ply of the laminate is meshed with one eight integration points 3D element in the thickness. The 3D element type used is C3D8I, which improves the behavior in bending, even with only one element in the thickness [16].

Only one element of 0.25 mm width is used to represent the whole width of the plate and plane strain conditions are assumed, making solution effectively 2D. This is consistent with experimental observations that show little variation across the width. The dimension of each element is 0.26 mm in the ply thickness and 0.25 mm in the other two directions.

To be able to predict delamination and splaying mode as observed during experiments, 8 nodes 3D cohesive elements (COH3D8) with zero thickness are used to model 0°/90° plies interfaces. The first interface element of each interface (i.e. at the specimen extremity) is removed to initiate delamination.

For each model, boundary conditions and loadings are imposed according to the experimental test as illustrated in Fig. 4. Nevertheless, to reduce the calculation time, only the first 80 mm of the length of the plate is modeled for dynamic plate crushing tests, which is considered long enough to represent the sliding of the plate inside the vertical guides. The rigid guides and the metallic base are modeled using analytical rigid bodies. For medium-scale quasi-static tests, only 35 mm of the specimen is represented with the first 5 mm being clamped (Fig. 4). Like in the experimental test, the unsupported length in Fig. 4a decreases as the imposed displacement increases. The constant loading speed in medium-scale static test modeling is artificially increased from 6 mm/min (experimental test) to 2 m/s to reduce the calculation time in the explicit simulations. This increase in speed should not affect the results of simulation, according to the results of the study of Duong et al. [14]. Using the same specimens, they found that the influence of crushing speed (from 20 mm/min to 9 m/s) on the energy absorption and force–displacement curve is relatively small. For dynamic plate crushing test modeling, an additional mass of 36 kg is added on the top nodes of the plate to represent the falling weight as imposed in the experimental test.

The mechanical input properties are listed in Table 1. They came from a series of identification tests [17–19] and from the manufacturer. Based on current simulation results, calculation times are approximately 2.5 h for medium-scale static model and 3.5 h for dynamic plate model, on 8 CPUs with parallel loops.

3.2. Modeling of fragmentation: free-face-crushing concept

According to the two different kinds of fragmentation observed in experiments – localized crushing and inside ply damage – it is essential that the simulation can represent these two mechanisms for a good prediction of the crushing morphology. In order to take into account the localized fragmentation, Matzenmiller et al. [20] introduced a concept of advancing crashfront. It consists in the use of a SOFT parameter which reduces the allowable strength of the elements in the crushing zone (only elements directly in contact with the impacted target). This concept has been implemented in Materials 54-55 of LS-Dyna and used to simulate the crushing of sinusoidal composite specimens [2] and square tubes [21]. The results of these simulations show that the deletion of elements leads to a series of unrealistic peaks in the load–displacement curve, which need to be filtered in post-processing. Moreover, the SOFT parameter is not related to any physical property.

To overcome such limitations, a similar free-face-crushing concept is introduced in the current model, coupled with a specific behavior law. In order to represent the localized crushing, with small debris and a constant mean crushing stress, elements at the extremity of plies (i.e. having free face in the direction of crushing) will have a different behavior than others. For elements behind, namely inside ply elements, classical failure criteria are applied.

The operating principle is illustrated in Fig. 5. Initially, only the element at the extremity of the ply is a free-face-crushing element (1). Subjected to compression, it will be crushed (see next paragraph for the localized crushing law applied). Once totally damaged, it will be deleted, and the element behind (2) will become a free-face-crushing element, and its behavior law will automatically change from inside ply to localized crushing law. Of course, the choice of this law is of first importance, as the use of discrete

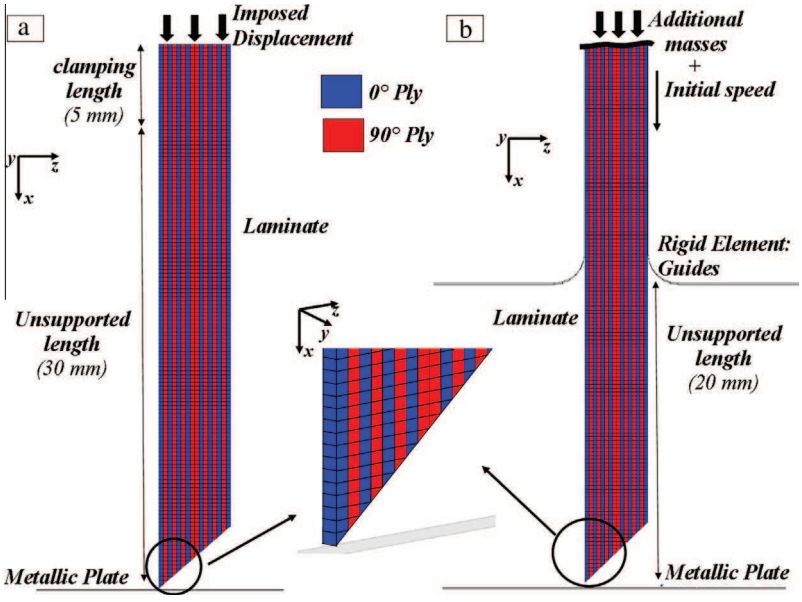

Fig. 4. Model lay-up: (a) medium-scale quasi-static (b) dynamic plate. (For interpretation of the references to colour in this figure legend, the reader is referred to the web version of this article.)

Table 1
Material properties of T700/M21 [17–19].

Parameters	Symbol	Values
Elastic data		
Density (kg/m^3)	ρ	1500
Longitudinal modulus		
Tensile (GPa)	E_{1t}	130
Compressive (GPa)	E_{1c}	100
Transverse modulus (GPa)	E_t	9
Shear modulus (GPa)	G_{1t}	5
Poisson's ratio	ν_{1t}	0.33
Material strength		
Transverse tensile strength (MPa)	Y^T	75
In plane shear strength (MPa)	S_C	110
Fiber failure (Mode I)		
Tensile strain at damage initiation	ε_t°	0.016
Compression strain at damage initiation	ε_c°	−0.012
Fracture toughness in tension (N/mm)	G_{1t}^f	133[a]
Fracture toughness in compression (N/mm)	G_{1c}^f	40[b]
Interface fracture toughness		
Mode I (N/mm)	G_I	0.6
Mode II/Mode III (N/mm)	G_{II}/G_{III}	2.1

[a] Extrapolated from material T300/913 ([18]).
[b] Estimated value in [19].

elements with deletion to represent a continuous mechanism leads to limitations in the model. This will be discussed further.

3.2.1. Localized crushing law

The implementation of a crushing criterion in the model, and especially in the free-face-crushing elements, is the main idea of this work. This criterion is based on the mean crushing stress (MCS) that a ply can sustain, for each direction (0° and 90°) [13]. The behavior (Fig. 6a) is similar to an elasto-plastic stress–strain constitutive law but only for the free-face-crushing elements in compression. The MCS of 0° plies (277 MPa) and 90° plies (270 MPa) used in this criterion are identified from characterization tests and are intrinsic parameters of the ply, independent from global parameters such as laminate lay-up, geometry and chamfering angle. Identification tests have been done under static conditions [15]. Results from plate crushing tests with different velocities performed by Duong et al. [14], show very small differences in the global plate behavior, which seems to indicate that the MCS is not dependent on the velocity (in the range of 0–10 m/s). Specific crushing tests to identify MCS should be carried out to verify this assumption.

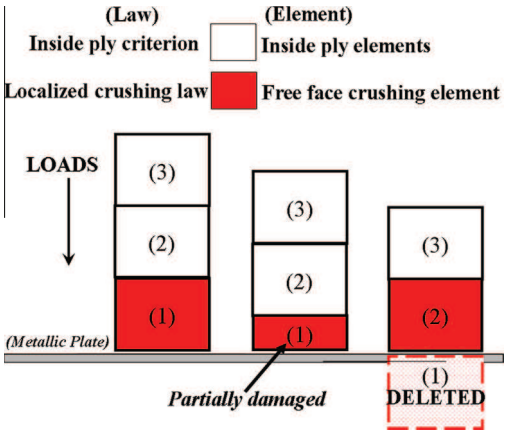

Fig. 5. Illustration of free-face-crushing concept. (For interpretation of the references to colour in this figure legend, the reader is referred to the web version of this article.)

The same type of criterion is also used by Greve et al. [9] in their phenomenological modeling based on Energy Absorbing Contact formulation and the results have showed good agreement with the experimental tests. However, their criterion depends on the global fragmentation stress of the laminate, obtained from a series of dynamic axial and oblique impact tests that makes it dependent on global parameters. As a consequence, the global fragmentation stress needs to be identified for each test configuration, which increases test costs and time consuming. The same limitation is also found in other phenomenological crush modeling like the CZone Abaqus crushing approach [10]. In addition, both phenomenological models mentioned here are suitable for larger scale composite structures, where the energy absorption is the only main motivation, and not the precise representation of damage occurring at sub-ply scale.

In the localized crushing law (Fig. 6a), the local crushing ($|\varepsilon| > \varepsilon^o$) starts when the compression stress of the element in the crushing direction reaches the MCS. Once the crushing is initiated, the element is compressed at the constant MCS until it reaches ε^c. The use of discrete elements, with deletion at the end, to represent the continuous crushing behavior raises the problems of excessive distortion before deletion and peak force release at deletion. To solve these problems, after reaching ε^c, a linear decrease of the stress is applied in order to smooth the force release, and the maximum allowable compression strain (ε^f) needed to delete the element is set to 95%. The localized crushing law is implemented in both 0° and 90° plies according to their local axis and MCS (Fig. 6b).

Unlike 0° plies in which small debris are continuously ejected from the crushing front, the debris wedge due to localized crushing in the 90° plies (Fig. 3) remains in the crushing front, and can instigate the delamination and splaying of adjacent 0° plies. Therefore, to represent this phenomenon, a pseudo-plastic deformation is imposed in the transverse direction (in laminate thickness or z-direction) of 90° plies, with a volume conservation rule to take into account the constant volume of the debris. However, even with a constant volume, the transverse expansion needs to be limited to avoid unrealistic expansion and premature delamination around the element. In practice, the expansion can be stopped after 15–45% compression without affecting significantly the results in terms of global crushing morphology. In this study, this transverse deformation is then stopped when the compression strain of the element in the loading direction reaches 40%, only to enable the initiation of an eventual splaying (Fig. 6c).

The pseudo-plastic transverse deformation law can be expressed as:

$$\Delta\varepsilon_{zz}^P = -\Delta\varepsilon_{tt}^P \quad \text{only true if} \quad |\varepsilon_{tt}^P| < \varepsilon_{40\%} \tag{1}$$

where ε_{tt}^P and $\Delta\varepsilon_{tt}^P$ are the plastic strain and plasticity increment of 90° element in the loading direction, while $\Delta\varepsilon_{zz}^P$ is the plasticity increment of 90° element in the laminate thickness.

3.2.2. Inside ply criterion

The inside ply criterion is implemented to simulate inside ply failure in inside ply elements (Fig. 5). This criterion is separated into two main failure modes: fiber failure and matrix cracking.

3.2.2.1. Fiber failure. Experimental observations show that most fiber failures are due to a combination of bending and compression in the 0° plies, leading to the two different modes of fiber rupture in the same ply: compression and tension, as shown in Fig. 7a. In addition, fiber breakages normally induce large energy release rates [18]. Thus, it is essential to take into account this energy to have a good prediction of the overall dissipated energy in the plate during crushing. For that reason, a fiber failure model developed by Bouvet et al. [22] is used in this work. They introduced an approach

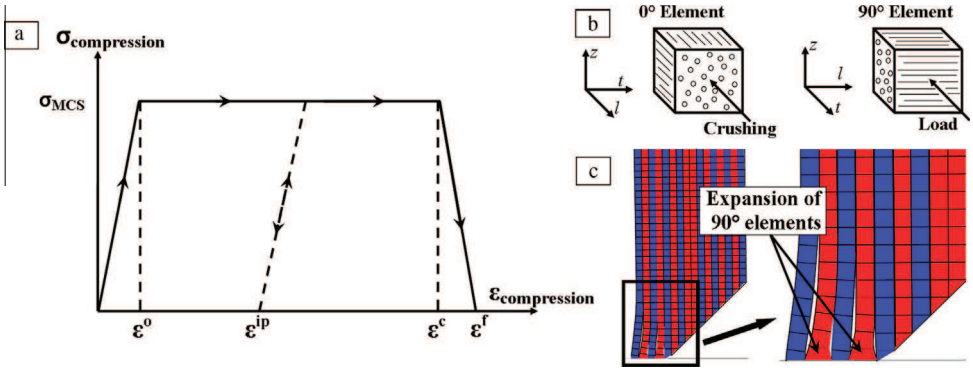

Fig. 6. (a) Localized crushing law (b) local axis of elements (c) 90° elements expansion in transverse direction. (For interpretation of the references to colour in this figure legend, the reader is referred to the web version of this article.)

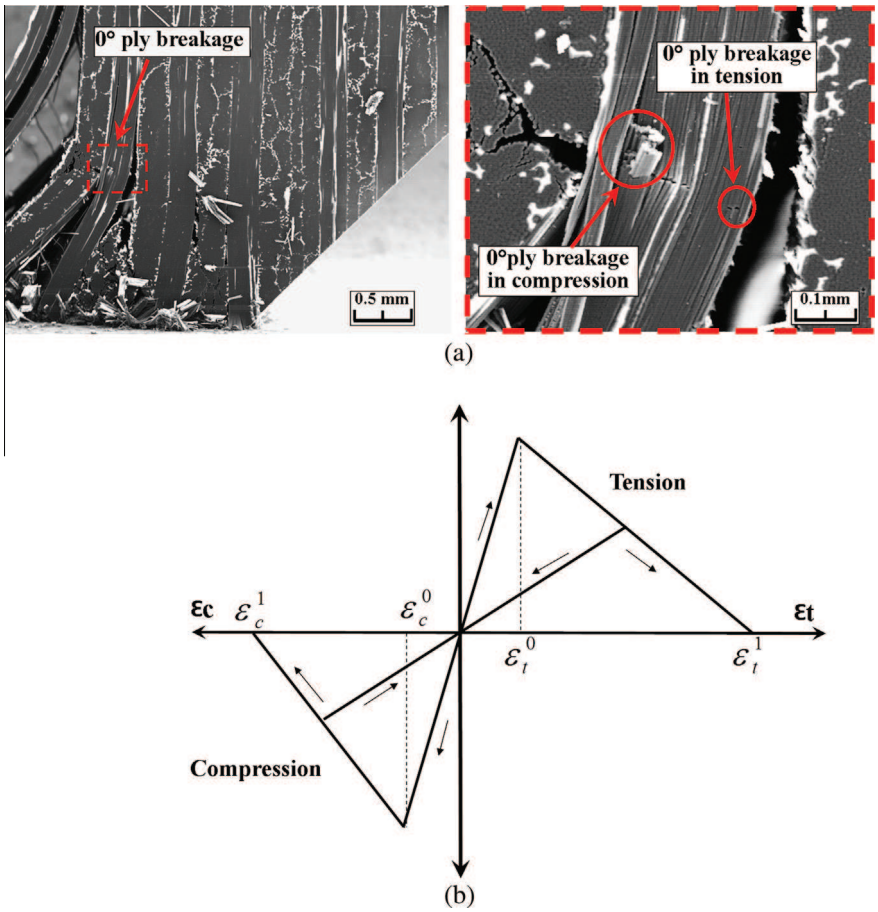

Fig. 7. (a) Ply breakage in bending (b) the fiber failure constitutive law. (For interpretation of the references to colour in this figure legend, the reader is referred to the web version of this article.)

to dissipate the fracture energy in an element defined as a function of the eight integration points. So, an energy release rate per unit area of crack can be obtained by dissipating energy throughout the volume of an element using the formulation in Eq. (2) based on crack band theory [23], with a characteristic element length. This approach enables to have a mesh-size independent model.

$$\int_V \left(\int_0^{\varepsilon^1} \sigma_l \cdot d\varepsilon_l \right) dV = S \cdot G_l^f \tag{2}$$

where $\sigma_l(\varepsilon_l)$, ε^1, S, V are the stress (strain) in the fiber direction, strain at full damage in the fiber direction, element's cross section normal to the fiber direction and element's volume, respectively. G_l^f is the fracture toughness for opening mode (mode I). Details of this criterion can be found in [19,22].

Besides that, this equation works even if tension and compression states occur at the same time in one element as shown in Fig. 7b, in order to represent bending behavior in the element: compression at certain integration points, tension for the others. Thus, at each time increment, the choice of damage calculation depends upon the critical loads, either in tension or compression and the damage evolution is computed taking into account the energy dissipated in both states (G_{lt}^f and G_{lc}^f have different values). (Once an element is fully damaged, it is deleted.)

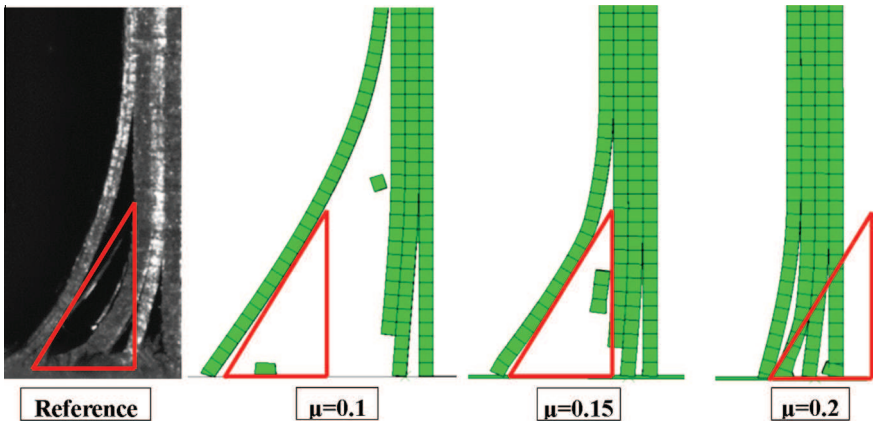

Fig. 8. Simulation for friction coefficient identification. (For interpretation of the references to colour in this figure legend, the reader is referred to the web version of this article.)

3.2.2.2. Matrix cracking. Matrix damage is essentially created by the transverse stress (σ_t) and the out-of-plane shear stress (τ_{tz}). Therefore, the following criterion is used to determinate the failure in 90° elements:

$$\left(\frac{\langle\sigma_t\rangle^+}{Y^T}\right)^2 + \left(\frac{\tau_{tz}}{S_C}\right)^2 = 1 \tag{3}$$

where $\langle\sigma_t\rangle^+$, τ_{tz} are the positive transverse stress and the shear stress in (tz) plane, respectively. Moreover, $\langle\sigma_t\rangle^+$ value is the maximum transverse stress among the eight nodes of each element, extrapolated from the eight integration points. While τ_{tz} is the average value of eight integration points. This is done to account for the bending behavior in elements. Damage evolution is not considered in this criterion since it induces very low energy compared to fiber failure, and can thus be neglected. Once the criterion reaches unity, the element is deleted.

The deletion of inside ply elements is important for the creation of macro-scale fragments (debris) during the simulation. However, it will cause a loss of mass and debris in the numerical model. Considering the size of debris in experiments compared to the size of an element, and the first simulation results, deletion of elements in these simulations seems acceptable.

3.3. Delamination

In this work, the classical traction–separation damage model in Abaqus software is used to govern the initiation and propagation of delamination between plies either in pure opening, shear or mixed-mode. This damage model [16] is basically derived from

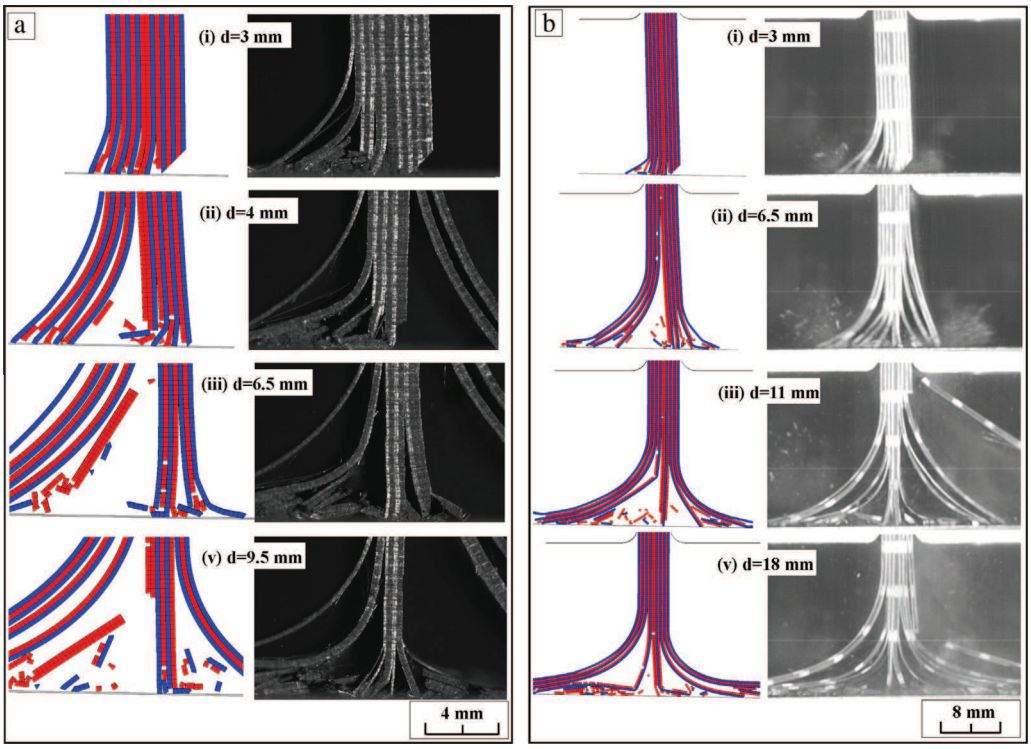

Fig. 9. Comparison of mixed-mode crushing morphologies between simulation and experiment (a) medium-scale quasi-static test (b) dynamic plate test. (For interpretation of the references to colour in this figure legend, the reader is referred to the web version of this article.)

fracture mechanics approach which considers the amount of energy required to create new fracture surfaces and has been developed based on a study by Camanho et al. [24]. The traction–separation law involves three states: a damage initiation, a damage evolution and a complete separation. Damage initiation is based on the quadratic nominal stress criterion presented in Eq. (4).

$$\left\{\frac{\langle\sigma_n\rangle}{\sigma_n^o}\right\}^2+\left\{\frac{\sigma_s}{\sigma_s^o}\right\}^2+\left\{\frac{\sigma_t}{\sigma_t^o}\right\}^2=1 \tag{4}$$

where σ_n, σ_s, σ_t are stresses normal to the interface, and in first and second shear directions.

The propagation of delamination is ruled by a linear decrease in the traction–separation law, and the mode mix phenomenon is also taken into account as a linear interaction between the three energy release rates (G_{ic}), expressed in Eq. (5).

$$\sum\frac{G_i}{G_{ic}}=1 \tag{5}$$

3.4. Contact

Friction plays an important role during crushing especially friction between the crushing surface and the metallic base (during splaying), and as friction relates to debris accumulation and debris wedge formation. The available general contact formulation with classical friction model based on Coulomb approximation is used to simulate the contact behavior between all exterior surfaces [16]. Since the friction coefficient has a great influence on the crushing process [6], it is necessary to have a good estimation of it.

The friction coefficient is identified from a series of elementary simulation tests (both static and dynamic models). Simulations are done with different friction coefficients from 0.05 up to 0.3. Then, for a given crushing displacement, the radius curvature and horizontal displacement of certain splaying plies are compared with experimental results, as presented in Fig. 8. Based on these simulations, friction coefficient $\mu = 0.15$ is set in both static and dynamic models. In this work, static and kinetic coefficients of friction are assumed to be the same.

4. Results and discussion

Two 0°/90° laminated plates are simulated under crushing with different loadings and boundary conditions. Fig. 9 presents the crushing morphologies of both static and dynamic models, compared with the experimental tests. Globally, the numerical models in both tests are able to represent the mixed crushing mode including all the major kinds of damage (splaying, localized crushing, inside ply failures and debris creations) and their coupling. The development of a specific wedge resulting from localized crushing of 90° elements in the numerical model is effective in initiating the delamination of 0°/90° interfaces and then drives the adjacent 0° plies to an eventual splaying. A stable progressive crushing due to localized crushing in central plies can be observed in both cases, as in the experiments (Fig. 9a(iii and iv) and b(iii and iv)).

In the model, for most of the fragments due to inside ply failure in 0° and 90° plies, the sizes are relatively close to the ones measured in experimental tests. For the medium-scale quasi-static model, the debris size is between 0.5 mm and 2.0 mm which is close to experimental results (0.5–2.5 mm), as can be seen in Fig. 9a. In dynamic plate tests, the size of debris is in the range from 0.5 mm to 5 mm for the experiments and 0.65 mm to 4.0 mm for the numerical model. This validates the choice made for the representation of fragments by the means of inside ply elements deletion.

While all major damage is well represented, during the transition phase from initiation to the progressive crushing, the numerical models show minor differences in terms of crushing morphology correlations. For example, in Fig. 9a(iii), the model simulates well the multiple delaminations on the right side as in the experimental test, but the delamination length is slightly under-predict in the numerical model. Consequently, both models have differences in the number of plies involved in splaying or localized crushing, compared to experiments (see Fig. 9a(iii and iv) and b(iii and iv)). Nonetheless, this does not affect much the result of force–displacement curve in numerical model. Crushing of composite plates involves significant displacements, rotations and geometric transformations that lead to large dispersion in global morphology of crushing processes, as verified experimentally. For example, the number of plies in fragmentation mode can vary significantly although tests are performed under the same conditions [13–15].

Force–displacement curves from models and tests are displayed in Fig. 10 for comparison. The curves from experiments and numerical model are comparatively close to each other which means that the main phenomena are well represented i.e. the curves initiation and the maximum forces obtained for both static and dynamic models are close with experimental results as a result of the implementation of localized crushing laws in the models. After that, both curves are flattened out to have steady crush load (plateau after peak force) as in experimental tests. One can observe small differences in the plateau level: 10.5% for the medium-scale quasi-static model and 10% for the dynamic plate model compared to the experimental tests. However, by taking into account the complexity of the fracture modes in the laminated plate crushing and the dispersion in tests, these small differences can be considered acceptable [6]. Furthermore, in order to reduce calculation

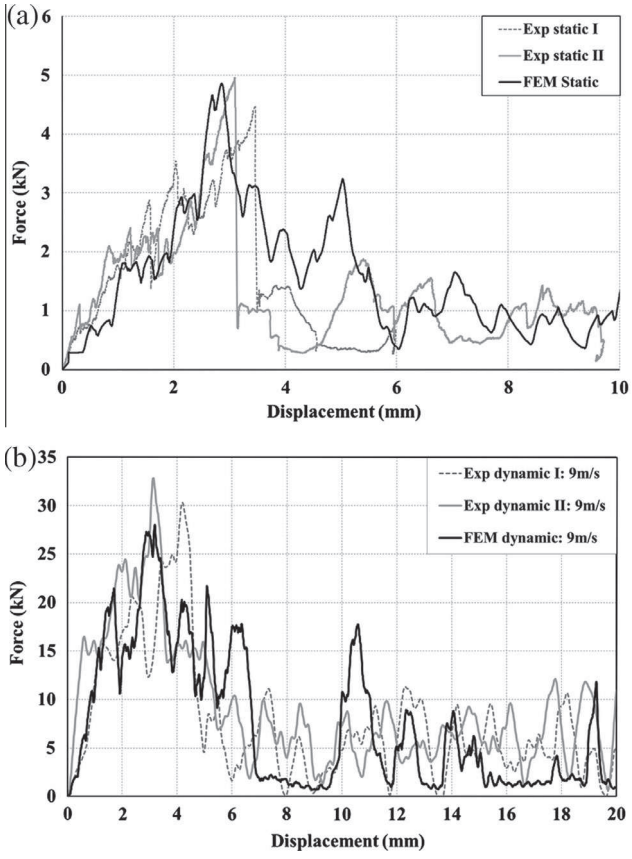

Fig. 10. Force displacement curves (a) medium-scale quasi-static test and (b) dynamic plate test (9 m/s).

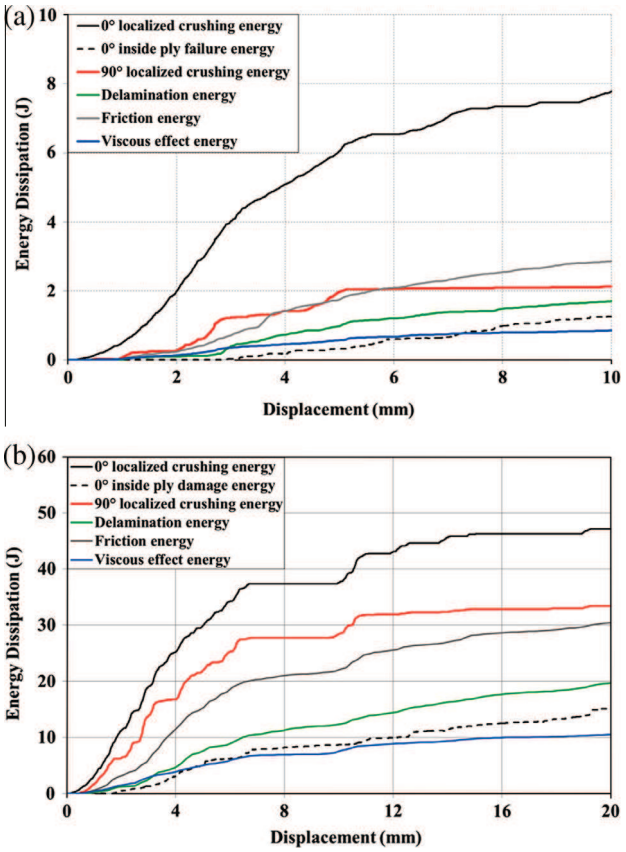

Fig. 11. The evolution of energy absorbed through various mechanisms during crushing tests of (a) medium-scale quasi-static and (b) dynamic plate crushing (9 m/s). (For interpretation of the references to colour in this figure legend, the reader is referred to the web version of this article.)

time, the numerical model for dynamic tests was solved for only the first 20 mm crushing length, which is considered enough to represent both initiation step and steady progressive crushing (plateau).

Results from the simulations also allow quantifying the contribution of each mechanism in energy absorption during the crushing tests: (a) 0° plies damage; (b) 90° plies damage; (b) delamination; (c) friction; and (d) viscous effect. Furthermore, the energy absorbed by 0° plies damage can be divided into two categories, which are energy absorbed via localized crushing and via inside ply failures. For 90° plies, the energy dissipated in inside ply failure is neglected, as assumed in Section 3.2.2.2.

The evolution of energy dissipation for each of these mechanisms during the crushing tests is presented in Fig. 11 for each test. In both cases, 0° plies damage mechanism via localized crushing absorb the highest part of the energy (49% and 30% of the total energy absorbed for static and dynamic tests, respectively) compared with the other mechanisms. This matches with the experimental observations that show the ability of 0° plies to perform a steady localized crushing throughout the crushing process while there are less inside ply failures (8% in static and 10% in dynamic tests). Although 90° plies have the same energy absorption ability as 0° plies (very close MCS), they dissipate less energy than 0° plies (13% in static test and 21% in dynamic test). This is due to the behavior of 90° plies that often turn into inside ply rupture due to their weakest strength compared to 0° plies. Thus, the volume of 90° plies involved in localized crushing is actually lower than in 0° plies during crushing.

The energy absorbed by friction is 17% and 19% of the total energy for static test and dynamic test respectively. Besides that, the delamination energy is significant and important to accurately capture the crushing morphology of mixed-mode crushing plate although it provides less energy absorption (10% in the static test and 13% in the dynamic tests, respectively).

5. Conclusion

The aim of this study is to propose a pseudo 2D finite element model for mixed-mode crushing in laminated plates subjected to low velocity crushing, depending only on the elementary material characteristics of the ply. Based on the presented results, the current development of the numerical model shows the capability to represent mixed-mode crushing for 0°/90° laminates with all major damages as observed experimentally. In addition, a good correlation is observed between the force–displacement curves from numerical models and experimental tests.

Despite some small differences in terms of crushing morphology, the main idea of this work is the introduction of a free-face-crushing concept in the model. This concept allows the use of two failure criteria at the same time in order to represent the phenomenology of localized crushing apart from classical inside ply failures. Furthermore, the implementation of the localized crushing law and the creation of a specific debris wedge in the 90° plies, free-face-crushing elements are capable to reproduce the complex localized damage mechanisms that occur at sub-ply scale and at all crushing modes (splaying and fragmentation) at the same time. Results from the simulation also allow making analyses of energy absorbed by each damage mechanism which is not possible during the tests. The results have demonstrated that localized crushing, especially in the 0° plies, dissipates the highest part of the total energy.

The next step of this work will be the extension of the same modeling strategy to a full 3D finite element model, including plies with orientations different from 0° or 90°.

Acknowledgements

Numerical simulations have been performed with the computing resources of CALcul en Midi Pyrénées (CALMIP, Toulouse-France). The authors also gratefully acknowledge the Ministry of Higher Education, Malaysia (MOHE) for the financial support of PhD program through the Aerospace Scholarship Scheme.

References

[1] Sokolinsky VS, Indermuehle KC, Hurtado JA. Numerical simulation of the crushing process of a corrugated composite plate. Composites Part A 2011;42(9):1119–26.
[2] Feraboli P, Wade B, Deleo F, Rassaian M, Higgins M, Byar A. LS-DYNA MAT54 modeling of the axial crushing of a composite tape sinusoidal specimen. Composites Part A 2011;42(11):1809–25.
[3] Xiao X, McGregor C, Vaziri R, Poursartip A. Progress in braided composite tube crush simulation. Int J Impact Eng 2009;36(5):711–9.
[4] Fleming DC, Morrow C, Clarke CW, Bird CE. Finite element simulation of delamination with application to crashworthy design. American Helicopter Society 62nd Annual Forum, Phoenix, May 2006.
[5] McGregor C, Vaziri R, Xiao X. Simulation of progressive crushing development in braided composite tubes under axial compression. Composites Part A 2007;38(11):2247–59.
[6] Pinho ST, Camanho PP, de Moura MF. Numerical simulation of the crushing process of composite materials. Int J Crash 2004;9(3):263–76.
[7] Farley GL, Jones RM. Energy-absorption capability of composite tubes and beams. NASA TM-101634, 1989.
[8] Mamalis A, Robinson M, Manolakos D, Demosthenous G, Ioannidis M, Carruthers J. Crashworthy capability of composite material structures. Compos Struct 1997;37(2):109–34.
[9] Greve L, Pickett AK, Payen F. Experimental testing and phenomenological modelling of the fragmentation process of braided carbon epoxy composite tubes under axial and oblique impact. Composites Part B 2008;39(7–8):1221–32.
[10] Nixon S, Barnes G. Effective crushing simulation for composite structures. ICCM-17, Edinburgh, UK, July 2009.

[11] Laurea ARM. Finite element investigations on the microstructure of composite materials. PhD thesis., University of Nottingham; 2007.
[12] Ladevéze P, Lubineau G. On a damage mesomodel for laminates: micro–meso relationships, possibilities and limits. Compos Sci Technol 2001;61(15):2149–58.
[13] Guillon D, Rivallant S, Barrau JJ, Petiot C, Thevenet P, Malherbe B. Experimental and numerical study of the splaying mode crush of CFRP laminates. ICCM-17, Edinburgh, UK, July 2009.
[14] Duong AV, Rivallant S, Barrau JJ, Petiot C, Malherbe B. Influence of speed on the crushing behavior of composite plates. ACCM-7, Taipei, Taiwan, November 2010.
[15] Israr HA, Rivallant S, Barrau JJ. Experimental investigation on mean crushing stress characterization of carbon-epoxy plies under compressive crushing mode. Compos Struct 2013;96:357–64.
[16] Abaqus 6.9 Analysis user's manual. Dassault Systèmes, 2009.
[17] Prombut P. Caractérisation de la propagation de délaminage des stratifiés composites multidirectionnels. PhD thesis, Université de Toulouse, 2007.
[18] Pinho ST, Robinson P, Iannucci L. Fracture toughness of the tensile and compressive fibre failure modes in laminated composites. Compos Sci Technol 2006;66(13):2069–79.
[19] Hongkarnjanakul N, Bouvet C, Rivallant S. Validation of low velocity impact modelling on different stacking sequences of CFRP laminates and influence of fibre failure. Compos Struct 2013;106:549–59.
[20] Matzenmiller A, Schwizerhof K. Crashworthiness simulations of composites structures – a first step with explicit time integration. In: Wriggers P, Wagner W, editors. Non-linear computational/mechanics – state of the art. Berlin: Springer-Verlag; 1991. p. 642–70.
[21] Mamalis A, Manolakos D, Ioannidis M, Papapostolou D. The static and dynamic axial collapse of CFRP square tubes: finite element modeling. Compos Struct 2006;74(2):213–35.
[22] Bouvet C, Rivallant S, Barrau JJ. Low velocity impact modeling in composite laminates capturing permanent indentation. Compos Sci Technol 2012;72(16):1977–88.
[23] Bazant ZP, Oh BH. Crack band theory for fracture of concrete. Mater Struct 1983;16:155–177Camanho PP, Davila CG, de Moura MF. Numerical simulation of mixed-mode progressive delamination in composite. J Compos Mater 2003;37(16):1415–38.
[24] Camanho PP, Davila CG, de Moura MF. Numerical simulation of mixed-mode progressive delamination in composite. J Compos Mater 2003;37(16):1415–38.